

Analysis of ICRF Heating by Three Dimensional Calculation in LHD

SEKI Tetsuo, KUMAZAWA Ryuhei, MUTOH Takashi, FUKUYAMA Atsushi¹, SAITO Kenji,
TORII Yuki², TAKEUCHI Norio², WATARI Tetsuo and LHD Experimental Group
National Institute for Fusion Science, Toki 509-5292, Japan

¹*Kyoto University, Uji 611-0011, Japan*

²*Nagoya University, Nagoya 464-8603, Japan*

(Received: 11 December 2001 / Accepted: 31 July 2002)

Abstract

Ion cyclotron range of frequency (ICRF) heating has been used in LHD and proved to be effective heating method for helical plasmas. For analysis of ICRF heating, full wave code has been used for toroidal plasmas. However, two-dimensional calculation, which has been carried out so far, is not sufficient for helical configuration. Then, development of three-dimensional calculation code has been started. In initial calculation, power deposition profile is similar to the experimental result. Dependence of power distribution on position of cyclotron resonance layer also agrees with the experiment.

Keywords:

ICRF heating, LHD, full wave code, TASK/WM, three-dimension

1. Introduction

Ion cyclotron range of frequency (ICRF) heating is one of the effective tools for plasma heating in magnetic-confined plasma experimental devices. In LHD, it is demonstrated that ICRF heating is also effective in helical device [1,2]. By ICRF heating, the profiles of the plasma parameters can be changed through change of the power deposition profile. Control of the profiles of plasma parameters is important for improvement of plasma confinement. Behavior of high-energy particles generated by ICRF heating is also important for understanding of plasma confinement and the related instabilities. Therefore, evaluation of ICRF heating is important for promoting the plasma confinement research of ICRF heated-plasmas.

To estimate the ICRF heating, global wave code has been used as one of the calculation codes. One-dimensional and two-dimensional codes have been used for tokamak and helical devices [3,4]. However, these

codes cannot include the complexity of magnetic field configuration and magnetic flux surface adapted in helical devices. These points are needed to consider in using the calculation result of these codes. Then, the calculation code based on more actual theoretical model is necessary. Due to progress of the computer technology in recent years, three-dimensional full-wave codes have been developed. TASK/WM code is one of three-dimensional full-wave code.

2. Coding of TASK/WM code

TASK/WM code is modeled by Vdovin et al. in ref. [5] and developed by Fukuyama. Plasma configuration is given by VMEC (Variational Moments Equilibrium Code) [6] and non-symmetric magnetic flux coordinate is used. Finite Larmor radius expansion is adopted and fast wave is mainly described. Toroidal and poloidal components of wave electric field are solved

Corresponding author's e-mail: seki@lhd.nifs.ac.jp

simultaneously. More details are described in followings.

2.1 Magnetic Flux Coordinates

Flux coordinates is non-orthogonal, i.e., the minor radius direction (poloidal magnetic flux) is defined as ψ , the poloidal direction is θ , and the toroidal direction is φ as shown in Fig.1. Co-variant expression of E is

$$\mathbf{E} = E_1 \mathbf{e}^1 + E_2 \mathbf{e}^2 + E_3 \mathbf{e}^3, \quad (1)$$

where contra-variant basis is

$$\mathbf{e}^1 = \nabla\psi, \quad \mathbf{e}^2 = \nabla\theta, \quad \mathbf{e}^3 = \nabla\varphi. \quad (2)$$

Jacobian is

$$J = \frac{1}{\mathbf{e}^1 \cdot \mathbf{e}^2 \times \mathbf{e}^3} = \frac{1}{\nabla\psi \cdot \nabla\theta \times \nabla\varphi}. \quad (3)$$

Metric tensor is $g_{ij} = \mathbf{e}_i \cdot \mathbf{e}_j$ and co-variant basis is $\mathbf{e}_i \equiv \partial\mathbf{r}/\partial x_i$.

2.2 Wave Equation

In full wave calculation, the wave equation is solved with poloidal and toroidal harmonic expansion. Maxwell's equation for stationary wave electric field E (angular frequency ω , light velocity c) is

$$\nabla \times \nabla \times \mathbf{E} = \frac{\omega^2}{c^2} \tilde{\epsilon} \cdot \mathbf{E} + i\omega\mu_0 \mathbf{j}_{ext}, \quad (4)$$

where $\tilde{\epsilon}$ is dielectric tensor including effects of finite temperature (cyclotron damping, Landau damping) and \mathbf{j}_{ext} is antenna current. Wave equation in non-orthogonal coordinates (radial components) is

$$\begin{aligned} (\nabla \times \nabla \times \mathbf{E})^1 = \frac{1}{J} \left[\frac{\partial}{\partial x^2} \left\{ \frac{g_{31}}{J} \left(\frac{\partial E_3}{\partial x^2} - \frac{\partial E_2}{\partial x^3} \right) \right. \right. \\ \left. \left. + \frac{g_{32}}{J} \left(\frac{\partial E_1}{\partial x^3} - \frac{\partial E_3}{\partial x^1} \right) + \frac{g_{33}}{J} \left(\frac{\partial E_2}{\partial x^1} - \frac{\partial E_1}{\partial x^2} \right) \right\} \right. \\ \left. - \frac{\partial}{\partial x^3} \left\{ \frac{g_{21}}{J} \left(\frac{\partial E_3}{\partial x^2} - \frac{\partial E_2}{\partial x^3} \right) \right. \right. \\ \left. \left. + \frac{g_{22}}{J} \left(\frac{\partial E_1}{\partial x^3} - \frac{\partial E_3}{\partial x^1} \right) + \frac{g_{23}}{J} \left(\frac{\partial E_2}{\partial x^1} - \frac{\partial E_1}{\partial x^2} \right) \right\} \right], \quad (5) \end{aligned}$$

where the coordinates is $(x^1, x^2, x^3) = (\psi, \theta, \varphi)$. Similar expressions hold for poloidal and toroidal components

2.3 Response of Plasmas

The dielectric tensor $\tilde{\epsilon}$ is usually described in Cartesian coordinates with static magnetic field along the z axis. The local normalized orthogonal coordinates is expressed as

$$\hat{\mathbf{e}}_s = \frac{\nabla\psi}{|\nabla\psi|}, \quad \hat{\mathbf{e}}_b = \hat{\mathbf{e}}_h \times \hat{\mathbf{e}}_\psi, \quad \hat{\mathbf{e}}_h = \frac{\mathbf{B}_0}{|\mathbf{B}_0|}. \quad (6)$$

Variable transformation, $\tilde{\mu}$ is defined as

$$\begin{pmatrix} E_1 \\ E_2 \\ E_3 \end{pmatrix} = \tilde{\mu} \cdot \begin{pmatrix} E_s \\ E_b \\ E_h \end{pmatrix}, \quad (7)$$

with

$$\tilde{\mu} \equiv \begin{pmatrix} \frac{1}{\sqrt{g^{11}}} & \frac{d}{\sqrt{Jg^{11}}} & c_2 g_{12} + c_3 g_{13} \\ 0 & c_3 J \sqrt{g^{11}} & c_2 g_{22} + c_3 g_{23} \\ 0 & -c_2 J \sqrt{g^{11}} & c_2 g_{32} + c_3 g_{33} \end{pmatrix} \quad (8)$$

and

$$\begin{aligned} c_2 = B^\theta/B, \quad c_3 = B^\varphi/B \\ d = c_2(g_{23}g_{12} - g_{22}g_{31}) + c_3(g_{33}g_{12} - g_{32}g_{31}) \\ g^{11} = (g_{22}g_{33} - g_{23}g_{32})/J^2. \end{aligned} \quad (9)$$

Dielectric tensor in non-orthogonal coordinates is $\tilde{\epsilon} = \tilde{\mu} \tilde{\epsilon}_{sbh} \tilde{\mu}^{-1}$.

2.4 Fourier Mode Expansion

Fourier mode expansion in poloidal and toroidal directions is utilized to solve the wave equation. Spatial variation of wave electric field, medium and, the left-hand side of Maxwell's equation are

$$\begin{aligned} E(\psi, \theta, \varphi) &= \sum_{mn} E_{mn}(\psi) e^{i(m\theta + n\varphi)} \\ G(\psi, \theta, \varphi) &= \sum_{lk} G_{lk}(\psi) e^{i(l\theta + kN_p\varphi)} \\ J(\nabla \times \nabla \times \mathbf{E}) &= G(\psi, \theta, \varphi) E(\psi, \theta, \varphi) \\ &= \sum_{m'n'} [J(\nabla \times \nabla \times \mathbf{E})]_{m'n'} e^{i(m'\theta + n'\varphi)}, \end{aligned} \quad (10)$$

where N_p is rotation number of helical coil in φ . Toroidal and poloidal modes are coupled separately and have following relations: $n' = n + kN_p$, $m' = m + 1$.

2.5 Parallel Wave Number

Plasma dielectric tensor $\tilde{\epsilon}(\psi, \theta, \phi, k_{\parallel}^{m''n''})$ depends on $k_{\parallel}^{m''n''}$ through the following plasma dispersion function $Z[(\omega - N\omega_{cs})/k_{\parallel}^{m''n''}v_{Ts}]$, where N is the cyclotron harmonic number and m'' and n'' are defined later in eq.(11). To account the effect of the poloidal magnetic field influence on k_{\parallel} wave number formation it is usually considered that the k_{\parallel} is the component of the spatial gradient in the direction of magnetic field. Then, we define k_{\parallel} as follows:

$$\begin{aligned} k_{\parallel}^{m''n''} &= -i\hat{e}_h \cdot \nabla = -i\hat{e}_h \cdot \left(\nabla\theta \frac{\partial}{\partial\theta} + \nabla\varphi \frac{\partial}{\partial\varphi} \right) \\ &= i\hat{e}_h \cdot \left(e^2 \frac{\partial}{\partial\theta} + e^3 \frac{\partial}{\partial\varphi} \right) = m'' \frac{B^\theta}{|B|} + n'' \frac{B^\varphi}{|B|} \end{aligned} \quad (11)$$

Fourier components of E in the local normalized orthogonal coordinates is expressed as

$$(J\tilde{\epsilon} \cdot E)^j = J\tilde{g}^{-1} \cdot \tilde{\mu} \cdot \tilde{\epsilon}_{sbh} \cdot \tilde{\mu}^{-1} \cdot E_j. \quad (12)$$

2.6 Boundary conditions

The plasma is assumed to be surrounded by perfectly conducting wall and vacuum region exists between plasma surface and the wall. In this boundary conditions on the conducting wall, tangential components of electric field vanishes. Co-variant expression is expressed as

$$\begin{aligned} E &= E_1 \nabla\psi + E_2 \nabla\theta + E_3 \nabla\varphi \\ E_2 &= 0, \quad E_3 = 0. \end{aligned} \quad (13)$$

For the boundary conditions on the magnetic axis ($\psi=0$), finiteness of the wave magnetic field and the induced charge density is utilized and they are expressed as follows:

$$\begin{aligned} m=0 & \quad \frac{\partial E_\varphi^{0n}}{\partial\psi} = 0 \\ m \neq 0 & \quad E_\varphi^{mn} = 0 \end{aligned} \quad (14)$$

Co-variant component E_θ^{mn} always vanishes on the axis.

2.7 Equilibrium calculation

VMEC (Variable Moments Equilibrium Code) is used as equilibrium solver. Cylindrical coordinates (R, ϕ, Z) shown in Fig.1 is expressed in terms of (ψ, θ, φ) as follows:

$$\begin{aligned} R &= \sum_{mn} R_{mn}(\psi) \cos(m\theta - n\varphi) \\ \phi &= \varphi \\ Z &= \sum_{mn} Z_{mn}(\psi) \sin(m\theta - n\varphi) \end{aligned} \quad (15)$$

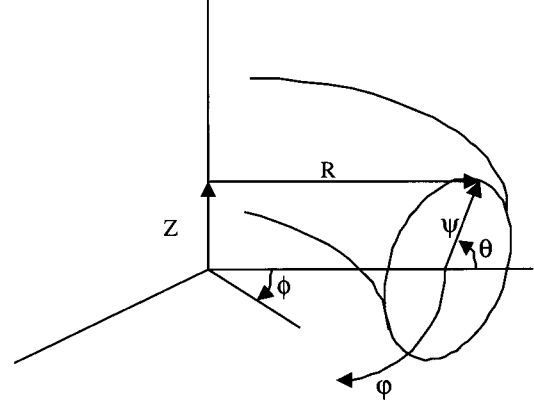


Fig. 1 Non-orthogonal and cylindrical coordinate systems.

Co-variant basis and metric tensor $g_{ij} = e_i \cdot e_j$ are expressed as follows, respectively;

$$\begin{aligned} e_1 &= \left(\frac{\partial R}{\partial\psi}, 0, \frac{\partial Z}{\partial\psi} \right) \\ e_2 &= \left(\frac{\partial R}{\partial\theta}, 0, \frac{\partial Z}{\partial\theta} \right) \\ e_3 &= \left(\frac{\partial R}{\partial\varphi}, \frac{\partial\phi}{\partial\varphi}, \frac{\partial Z}{\partial\varphi} \right) \\ g_{11} &= \left(\frac{\partial R}{\partial\psi} \right)^2 + \left(\frac{\partial Z}{\partial\psi} \right)^2 \\ g_{12} &= \left(\frac{\partial R}{\partial\psi} \right) \left(\frac{\partial R}{\partial\theta} \right) + \left(\frac{\partial Z}{\partial\psi} \right) \left(\frac{\partial Z}{\partial\theta} \right) \\ &\dots \\ J &= R \left(\frac{\partial R}{\partial\psi} \frac{\partial Z}{\partial\theta} - \frac{\partial Z}{\partial\psi} \frac{\partial R}{\partial\theta} \right) \end{aligned} \quad (16)$$

Finite difference method in ψ is adopted and linear mesh with respect to ρ is used. Where ρ is $\rho = \sqrt{\psi/\psi(\text{surface})}$. They are numerically solved by the band matrix equation.

3. Calculation Results

Figure 2 shows the profile of hydrogen absorbed power at the poloidal cross section. Helium majority and hydrogen minority plasma is assumed. The electron density is $1 \times 10^{19} \text{ m}^{-3}$ and the temperature is 1.5 keV. Ion cyclotron resonance layer of hydrogen is also plotted. The position of the layer is same as the experimentally optimized place. In two-dimensional calculation, absorbed hydrogen power concentrated at the vicinity of the cyclotron layer. However, it is spread in the flux surface in the three-dimensional calculation.

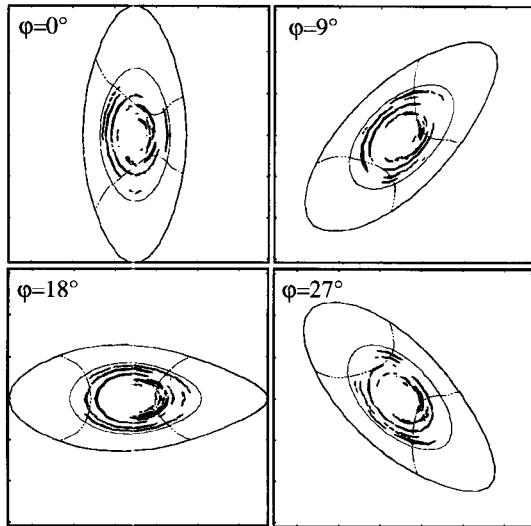


Fig. 2 Deposition profile of minority ions (hydrogen) at the poloidal cross section. The ion cyclotron resonance layer is also plotted.

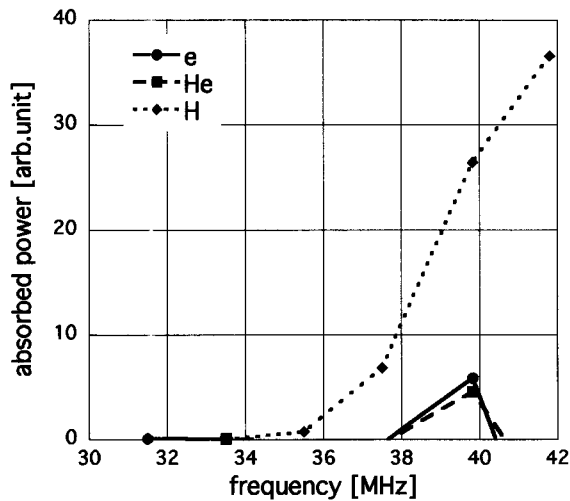


Fig. 3 Dependence of power distribution on wave frequency. Solid line, dashed line, and dotted line correspond to electrons, minority ions (helium), and minority ions (hydrogen), respectively.

Figure 3 shows the power distribution as a function of wave frequency. The cyclotron resonance layer is located at the magnetic axis around 42 MHz and the plasma edge at 31.5 MHz. The ratio of power absorption by hydrogen ions is increased as the cyclotron resonance layer approaches to the magnetic axis. This tendency was observed in the experiment. The power absorption by helium and electron is very small compared to the

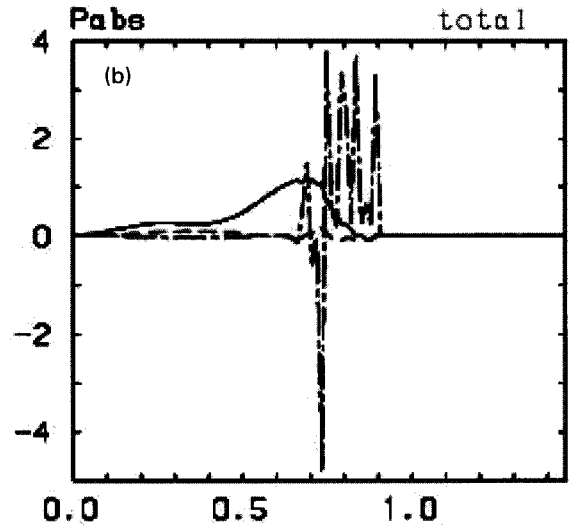
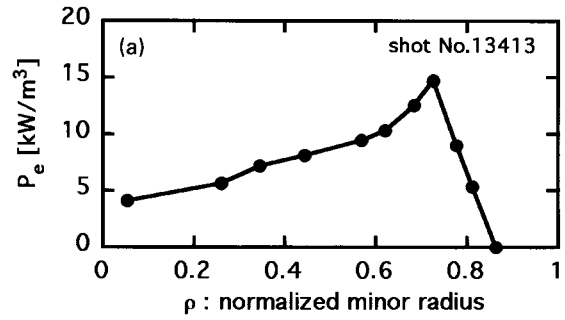


Fig. 4 Radial deposition profile. (a): The experimental result. Only electron absorption; (b): The calculation result. Solid line, dashed line, and dashed-dotted line correspond to electrons, majority ions (helium), and minority ions (hydrogen).

hydrogen absorption.

Figure 4 shows the radial profile of the power deposition obtained by the experiment [2] and the calculation. In the experiment, only electron absorption is shown. The ion cyclotron resonance layer is located near the plasma edge in this case. The ion absorption is very weak. Then, it is difficult to tell about the ion absorption in this case. Concerning to the only electron absorption, the peak is located at around the $\rho=0.7$ and almost same shape of profile is obtained in the experiment and the calculation.

4. Summary

To study the ICRF heating in helical device, three-dimensional full wave code, TASK/WM, was developed and applied to the LHD plasma. In the initial calculation, dependence of ion absorption on the

position of the cyclotron layers is studied and the electron absorption profile in the case that electron heating is dominant is obtained. The study has just begun and more parameter scan can be necessary.

References

- [1] T. Seki *et al.*, *Controlled Fusion and Plasma Physics (Proc. 27th Eur. Conf. Budapest, 2000)* European Physical Society (2000) CD-ROM.
- [2] K. Saito *et al.*, *Nucl. Fusion* **41**, 1021 (2001).
- [3] A. Fukuyama *et al.*, *Nucl. Fusion* **23**, 1005 (1983).
- [4] E.F. Jaeger *et al.*, *Nucl. Fusion* **30**, 505 (1990).
- [5] V.L. Vdovin *et al.*, NIFS-469 (1996).
- [6] S.P. Hirshman *et al.*, *Comp. Phys. Comm.* **39**, 161 (1986).